Journal of Applied Polymer Science

Effect of Solvents on Morphology and Polymorphism of Polyvinylidene Fluoride Membrane via Supercritical CO_2 Induced Phase Separation

Yanhui Xiang, Lixin Xue, Jianhui Shen, Haibo Lin, Fu Liu
Ningbo Institute of Materials Technology & Engineering, Chinese Academy of Sciences, Ningbo 315201, China
Correspondence to: F. Liu (E-mail: fu.liu@nimte.ac.cn) and L. Xue (E-mail: xuelx@nimte.ac.cn)

ABSTRACT: Poly vinylidene fluoride (PVDF) membranes were prepared via supercritical CO_2 induced phase separation. The effects of solvent power on PVDF membrane morphology and polymorphism were investigated using *N*-*N*-dimethylformamide (DMF), triethyl phosphate (TEP), and their mixture respectively. The morphology evolution including cross-section and surfaces were thoroughly studied by scanning electron microscope (SEM) and atomic force microscopy (AFM). The differences of solubility parameters between the solvent and PVDF affected the phase separation and the resultant morphology. The various crystalline phases of the membranes were mainly investigated by Fourier transform infrared spectroscopy (FTIR) and X-ray diffractometer (XRD). Solvent with larger dipole moment tended to form polar β phase. Decreasing the difference of solubility parameters favored the formation of α phase. Furthermore, the effects of salt additive on PVDF membrane morphology and crystalline form were studied as well. Results turned out that lithium chloride (LiCl) induced a porous top surface and boosted the formation of β phase. © 2014 Wiley Periodicals, Inc. J. Appl. Polym. Sci. **2014**, *131*, 41065.

KEYWORDS: membranes; morphology; porous materials

Received 2 April 2014; accepted 20 May 2014
DOI: 10.1002/app.41065

INTRODUCTION

In recent years, poly vinylidene fluoride (PVDF) has been widely applied to produce ultrafiltration and microfiltration membranes due to its high mechanical strength, thermal stability, chemical resistance, and high hydrophobicity.[1–5] The majority of PVDF ultrafiltration and microfiltration membranes are prepared by nonsolvent induced phase separation (NIPS)[6] and thermally induced phase separation (TIPS).[7] During both membrane methods, plenty of organic solvents and low molecular weight diluents are applied. Unfortunately, most of them are flammable, volatile, and may pose a risk to health and environment. Therefore, the organic solvents and dilutes must be expensively removed from membrane by post treatments, especially in the case of biomedical and pharmaceutical applications. Alternative membrane preparation approaches are being developed, among them supercritical CO_2 induced phase separation attracts much attention.[8–10] As a supercritical fluid, supercritical CO_2 has a low viscosity and high diffusivity and is miscible with a lot of organic solvents.[11] Compared with traditional phase inversion process, the advantages of the novel technique are noticeable. Because of the absence of a liquid-vapor interface, porous membranes can be prepared without collapse of structure; supercritical CO_2 not only induce phase separation but also dry the formed membrane meanwhile; the organic solvent dissolved in supercritical CO_2 allows to be extremely removed by simply diminishing the pressure.[12]

Generally speaking, polymer crystallinity and the resultant membrane morphology are among important factors in determining the physical and chemical properties of membrane. It is widely accepted that, PVDF chains can crystallize into at least four distinct phases or forms, which are α (form II), β (form I), γ (form III), and δ (form IV).[13,14] Usually α and β phase, belonging to monoclinic and orthorhombic crystalline system, respectively are reported and identified. The nonpolar α phase with molecular chain conformation of trans-gauche (TGTG′) placing H and F atoms alternately on each side of the chain is usually obtained from melt crystallization or solution deposition. The polar β phase, with all trans planar zigzag conformation (TTT) is attractive for its piezo-, pyro-, and ferroelectric properties.[15–17] Crystallization of PVDF membrane is controlled by a number of variables including the concentration of casting solution, supercritical processing condition, solvent power,[18] and the additives in solution dope.[19] Previous research has found out that one crystalline phase could also be converted to another one by appropriate thermal, mechanical, or electric treatments.[20,21]

Enrica Fontananova found out that PVDF membrane morphology and transport properties could be modified by additives in the casting solution during NIPS method.[22] In particular, it was

found that polyvinylpyrrolidone improves membrane permeability; LiCl can be used in order to reduce macrovoids formation and increase the mechanical stability of the membranes. The effect of crystallization rate on polymorphs of solution cast PVDF was investigate by Rinaldo Gregorio and it was found that low rates result predominantly in β phase, high rates predominantly in α phase.[23]

Despite a number of researches have been carried out to understand the polymorphism of PVDF membrane, most of them focused on NIPS process. To the best of our knowledge, the study of the solvent power and inorganic salt on PVDF membrane polymorphism and crystallization behavior during supercritical CO_2 induced phase separation has not been reported. In this article, all experiments were carried out at a fixed PVDF casting content (18 wt %) and supercritical condition (45°C, 80 bar). *N*-*N*-dimethylformamide (DMF), triethyl phosphate (TEP), and the mixture of the two reagents with different ratios were used as solvents with different solvent power. The impact of LiCl on the crystallization was also investigated.

EXPERIMENTAL

Materials

PVDF (FR904) was supplied by Shanghai 3F New Material, Ltd. China. Anhydrous LiCl was supplied by Shanghai Aladdin Chemistry, Ltd. China. They were dried at 80°C in a vacuum oven for 24 h before use. Analytical reagent DMF and TEP which used as solvents for PVDF were supplied by Sino pharm Chemical Reagent, Ltd. China. Carbon dioxide with a purity of 99% was supplied by Wanli Gas of Ningbo, China. All chemicals were used as received.

Membrane Preparation

The experimental apparatus used in our study was similar to that described by Matsuyama et al.[24,25] Eighteen percent by weight PVDF with or without salt additive (LiCl) was dissolved in different solvents including DMF, TEP, and their mixture. LiCl concentration investigated was 1, 2, and 4 wt %, respectively. The casting solution was dissolved at 60°C and stirred at a constant speed for 24 h to achieve a homogenous solution, which was subsequently kept still overnight to remove air bubbles and then cast uniformly onto a clean polyimide film (diameter = 30 mm). The scraper clearance was controlled as 200 μm. Afterwards the polyimide film was rapidly transferred into a high pressure vessel, which was preheated to 45°C. This process was finished within 1.5 min for the sake of solution evaporation. The vessel was immediately filled with CO_2 until required pressure as soon as the sealing was accomplished. The system was held for 1 h at constant temperature and pressure, and thereafter performed in a continuous mode to sweep CO_2 through the cell to dry the phase separated polymer solution for 2 h. During this sweeping process, supercritical CO_2 was used as an extraction reagent to remove the solvents from the membrane. Finally, the vessel was slowly depressurized for about 1 h to collect white and opaque membrane.

Membrane Characterization

Morphological structures of the prepared PVDF membranes were examined by scanning electron microscope (SEM, S-4800, Hitachi, Japan) with an accelerating voltage of 4.0 kV and 7 μA. The cross-section of the membranes was fractured in liquid nitrogen. Both surface and cross-section of the samples were gold sputtered for 2 min before observation.

An atomic force microscopy (AFM, Veeco Dimension 3100V, US) was also used to further study the surface topography of the membranes. All membranes were fixed on the magnetic disk and then attached to a magnetic sample holder, finally located on top of the scanner tube. The laser beam of the AFM was focused on the preselected spot of the surface prior to the engagement of the cantilever. AFM images were carried out in the tapping mode with silicone tip cantilevers having a force constant of 20 mN/cm.

The crystalline form of the membrane bulk was detected by an X-ray diffractometer (XRD, D8 Advance, Bruker, Germany), using Cu Kα radiation, with the generator working at 40 kV and 40 mA. All samples were analyzed in a continuous scan mold between 10° and 60° 2θ with the scanning speed of 0.2 s/step.

Fourier transform infrared spectroscopy (FTIR, Thermo Nicolet 6700, US) over a range of 4000–400 cm^{-1}. To obtain the crystalline phase of top surface of PVDF membrane, FTIR spectrometer in mold of the attenuated total reflectance (FTIR-ATR) was adopted. The penetrations depth d can be estimated as[26]:

$$d = \frac{1}{2\pi n_c \sigma \left(\sin \vartheta^2 - n_x^2\right)^{1/2}} \quad (1)$$

Assuming both the refractive index n_c of ATR crystal and the ratio n_x between refractive indexes of sample and ATR crystal are constant in the considered frequency range. Moreover, σ is the wave number, ϑ is the angle of incidence. Here, ϑ is 45°, the refractive index of PVDF and ATR crystal are assumed to be 1.5 and 2.4, respectively.

The melt temperature and crystallinity of the formed membranes were determined by differential scanning calorimeter (DSC, Pyris Diamond, Perkin Elmer, US) equipped with a cooling apparatus under a nitrogen atmosphere at a heating rate of 10°C/min over the range of 30–250°C. Approximately 5.0 mg sample was sealed in an aluminum pan and placed in heating chamber together with an empty pan witch was used as a reference. Melting temperature (T_m) and heat of fusion (ΔH_f) were determined from the melting endotherms. Crystallinity of membrane was calculated by dividing the measured ΔH_f by the value of perfect PVDF crystal ($\Delta H_0 = 105$ J/g) reported in Ref. 27.

The hydrophilicity of formed membranes was evaluated by water contact angle measurement using a contact angle meter (OCA20, Dataphysics, Germany). During the measurement, 2 μL deionized water was dropped onto the top surfaces of membranes using a micro-syringe automatically. Each membrane was measured at least 5 times from different surface locations, and the mean value was calculated.

Solubility Parameter Calculations

Affinity between solvents and polymers can be described by introducing the "solubility parameter," δ, which is defined as square root of cohesive energy density and depicts the distance

Table I. Solubility Parameter and Dipole Moment of the Solvents Used

Sample name	Solvent composition	$\delta_{s,d}$ MPa$^{1/2}$	$\delta_{s,p}$ MPa$^{1/2}$	$\delta_{s,h}$ MPa$^{1/2}$	δ_s MPa$^{1/2}$	$\delta_{p,s}$ MPa$^{1/2}$	Dipole moment (D)
M-DMF	DMF	17.4	13.7	11.3	24.8	2.43	3.82
M-D7T3	DMF/TEP(7/3)	17.2	13.0	10.67	24.06	1.55	3.60
M-D5T5	DMF/TEP(5/5)	17.1	12.6	10.3	23.6	1.06	3.45
M-TEP	TEP	16.8	11.5	9.2	22.3	1.08	3.07

between polymer and solvent in a three-dimensional Hansen space. Interactions between polymer and solvents can be evaluated on the basis of the difference of solubility parameters. The solubility parameter (δ) of liquids and polymers can be defined as[28]:

$$\delta=\sqrt{\delta_d^2+\delta_p^2+\delta_h^2} \quad (2)$$

where δ_d, δ_p, and δ_h denote the contributions of dispersive interactions (d), polar bonding (p), and hydrogen bonding (h), respectively.

The solubility parameter of the mixed solvents can be calculated based on the volumetric average of the δ values of the pure compounds[29]:

$$\delta_i=\frac{X_1V_1\delta_{i,1}+X_2V_2\delta_{i,2}}{X_1V_1+X_2V_2},\ i=d,p,h \quad (3)$$

where δ_i is the solubility parameter of the mixed solvent, X is the molecular fraction, V is the molecular volume, and 1 and 2 stand for the two sorts of solvents, respectively.

The difference of solubility parameters between solvents and polymer is calculated using the equation:

$$\delta_{p,s}=\sqrt{(\delta_{p,d}-\delta_{s,d})^2+(\delta_{p,p}-\delta_{s,p})^2+(\delta_{p,h}-\delta_{s,h})^2} \quad (4)$$

where P and S represent the polymer and solvent. The solubility of PVDF is $\delta_p=23.2$ MPa$^{1/2}$ and the dispersive interactions (δ_d), polar bonding (δ_p), and hydrogen bonding (δ_h) parameters are 17.2, 12.5, and 9.2 MPa$^{1/2}$, respectively.[30]

The smaller difference between the solubility parameters of polymer and solvent means the stronger dissolving capacity of solvent. Table I shows the composition of the solvent and solubility parameter disparity of PVDF and solvent.

RESULTS AND DISCUSSION

Effect of Solvent Power on Membrane Characteristics

During supercritical CO_2 induced phase separation, the precipitation occurs because of the exchange of solvent and nonsolvent (supercritical CO_2), the suitable choice of pairs of solvents is a very important parameter to control the polymorphism of prepared membranes. The scope of this part was focused on the solvent power on PVDF membrane morphology and crystalline form. The solvent power was regulated by the ratio of DMF and TEP mixture.

Morphology of PVDF Mmembranes Prepared with Different Solvent Compositions. Figure 1 shows the cross-section and surface structure of membranes prepared with different solvent compositions. From the whole cross-section, all membranes exhibited a combination of dense and loose spongy like pores, and finger like pores were completely depressed with regard to a fast exchange between solvent and nonsolvent. Supercritical CO_2 has a similar density with liquid whereas the viscosity is only hundredth, thus during the supercritical CO_2 induced phase separation, the mutual diffusion between solvent and nonsolvent is much faster as compared to that in NIPS method. In this case, the polymer concentration in polymer rich phase rapidly evolved into solidification region, freezing the finger like pores or macrovoids, and therefore a spongy like pore or cellular pore forms.[31,32] As increasing the amount of TEP in solvent, the pore size of loose cross-section decreased from 2–3 μm to $\sim$1 μm. This variation is related to solvent viscosity, introducing TEP enhanced the solution viscosity and hindered the inflow of supercritical CO_2.

All membranes exhibit a porous top surface except for M-D5T5. The appearance of skin layer is related to polymer concentration gradient, which is caused by the evaporation of solvent before and after contacting with supercritical CO_2. Because of the rapid loss of solvent from top surface, an increased polymer concentration is created near top surface to cause a quick precipitation and dense skin layer. It was pointed that the formation of skin layer produced from different solvents is controlled by the equilibrium thermodynamics, whereas the sub-layer structure is dominated by the diffusion rate of solvent and nonsolvent.[33] It is widely accepted that, a decrease of $\delta_{p,s}$ means an increase of soluble power of solvent, and more stable casting solution was formed.[30,34] In case of M-D5T5, $\delta_{p,s}$ of the mixed solvent was only 1.06 MPa$^{1/2}$, demonstrating a great dissolving capacity for PVDF, and the phase separation was therefore delayed and a nonporous dense top surface was formed consequently. The bottom surface of membranes became much rougher and porous with adding TEP. The thickness of membranes prepared with different solvents varied obviously (Figure 1 and Table II). M-DMF and M-TEP produced with pure solvents obtained a larger thickness than M-D7T3 and M-D5T5.

The feature of top surface is one of the very important characteristics of membrane. For this reason, AFM experiment was carried out. The result in Figure 2 shows that M-DMF and M-D5T5 had a similar top surface roughness, the arithmetic roughness (Ra) was around 140 nm. Whereas M-D7T3 and M-TEP obtained much rougher surface, both of them achieved a Ra over 200 nm, which was in accordance with SEM experiment, a plenty of pores were obtained in top surface of M-D7T3 and M-TEP.

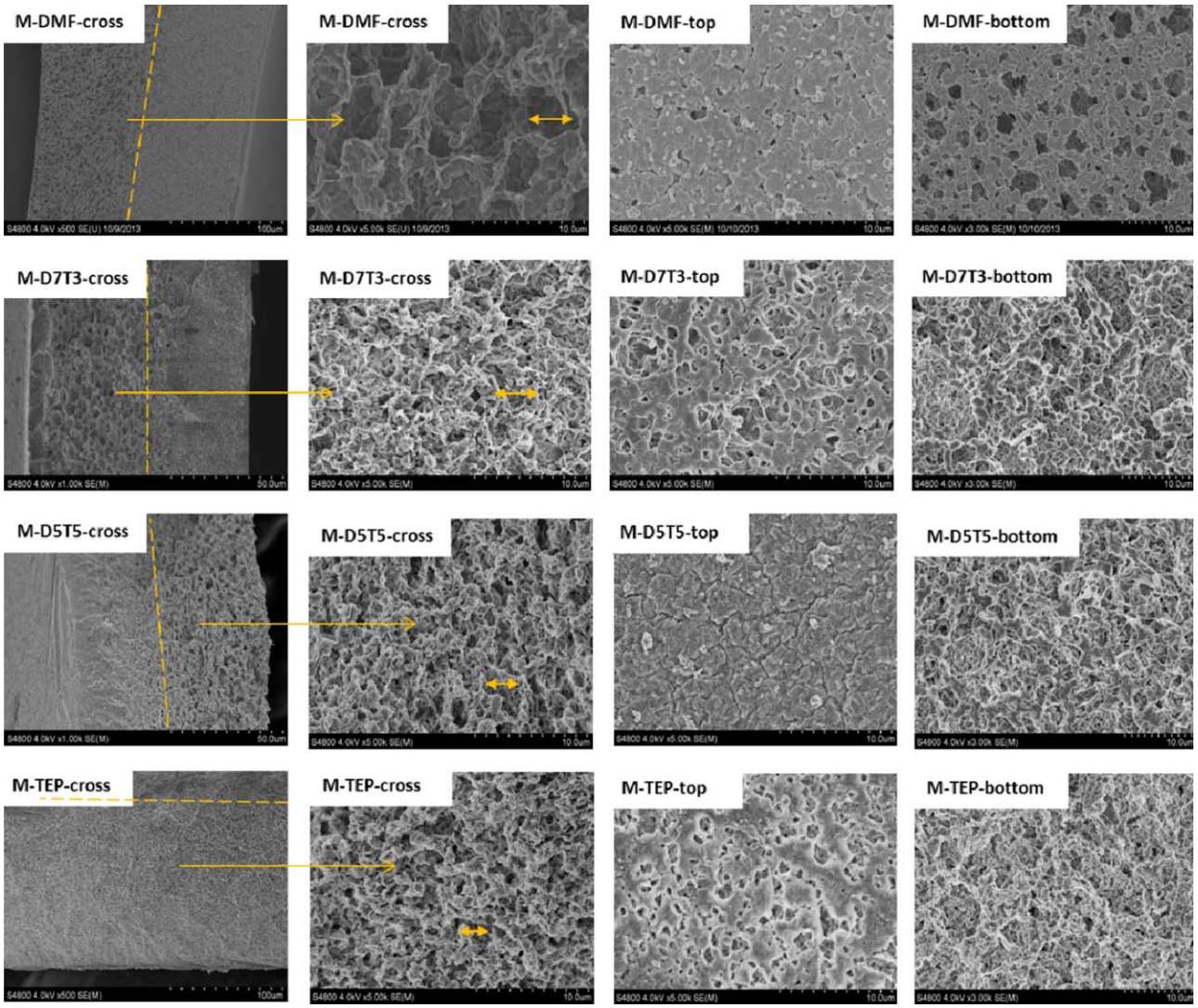

Figure 1. SEM images of cross-section and surface structures of M-DMF, M-D7T3, M-D5T5, and M-TEP. [Color figure can be viewed in the online issue, which is available at wileyonlinelibrary.com.]

Crystalline Structure of PVDF Membrane Bulk by FTIR and XRD. Crystallographic data available from literature for phases analysis are however sometimes ambiguous. Usually, α and β phase are reported and identified. In our study, we focus on these two crystalline forms, and analysis from a qualitative point of view. FTIR and XRD methods were applied to study the polymorphic behavior of PVDF membrane bulk. Figure 3 shows that β characteristic peaks at 511 and 840 cm^{-1} could not be observed for M-D5T5 and M-TEP. However, peak at 531 cm^{-1}, typical of α phase, was relatively sharper. It was obvious that the signals of β phase at 511 and 840 cm^{-1} were in strong intensity for M-DMF. As adding TEP, β phase signal of M-D7T3 was weakened. Particularly, for M-D5T5 and M-TEP, none signal of β phase could be identified. To further verify the result from FTIR, XRD experiment was then carried out. As shown in Figure 4, M-DMF presented a strong peak at 20.5° in the region 15°–25°, which actually came from the superposition of β (200) and β (110) reflection. In addition, there was a small shoulder at 18.6° accompanying the peak, which could be attributed to α (020) reflection. This overlap around $2\theta = 20°$

Table II. Properties of the PVDF Membranes Prepared with Different Solvent Composition

Sample name	Thickness (μm)	Contact angle (°)	T_m (°C)	Crystallization (%)
M-DMF	185	108	164.6	37.8
M-D7T3	88	110	163.7	40.8
M-D5T5	98	122	165.3	40.8
M-TEP	162	112	163.9	39.3

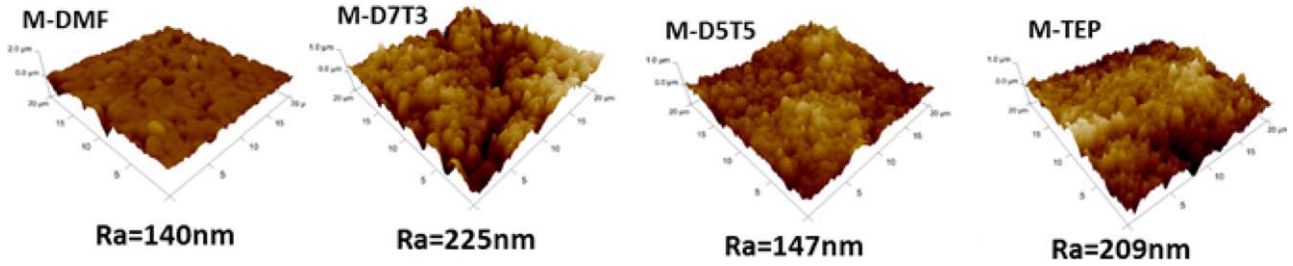

Figure 2. Three-dimensional AFM images of M-DMF, M-D7T3, M-D5T5, and M-TEP. [Color figure can be viewed in the online issue, which is available at wileyonlinelibrary.com.]

was resulted from the simultaneous presence of α and β phase. The wide peak around 40° referred to α (002) and α (201). Compared with M-DMF, M-D7T3 had a distinct shoulder peak at 18.6°, furthermore, weak peak α (002) between 25° and 30° became visible. Both of them indicated an increase of α phase for M-D7T3. In general, M-DMF and M-D7T3 obtained a crystalline forms combined of α and β phase, and β phase was predominantly. Unlike M-DMF and M-D7T3, the peak α (020) at 18.6° for M-D5T5 and M-TEP became apparently evident. Specifically for M-TEP, the shoulder peak seemed completely apart from the main peak at 20.5° and the membrane had a typical α phase. Moreover, peaks around 26.5° and 40° ascribed to α phase appeared sharp and apparent. All results came to a conclusion that increasing the amount of TEP in solvent favored the formation of α phase.

To better understand the membrane crystalline form evolution, the solvents dipole moments should be accounted. It was found that dipolar interaction at interface between PVDF nucleus and solvent molecules can preferably lead to trans conformation packing of CH_2—CF_2 dipoles, thus β phase is formed during crystallization.[35,36] Dipole moments of the four solvents used in our experiment were listed in Table I. According to this theory, the content of β phase in above four systems should decrease in the same order as the polarity variation: M-DMF > M-D7T3 > M-D5T5 > M-TEP. The experimental results agreed well with this assumption. DMF gained a largest dipole moments value, in this case, polar PVDF chain tended to orient and polar β phase was favored. When TEP with low polarity was applied as the solvent, polar PVDF chain was dissolved in a random way and it needed high energy and long time to form all trans molecular conformation. In this case, α phase was preferable to β phase and almost none β type could be found in M-TEP bulk.

Another interpretation was from the point of solubility parameter ($\delta_{p,s}$) between solvent and polymer. For DMF, $\delta_{p,s}$ was 2.43 $MPa^{1/2}$, whereas the ratio of DMF and TEP in mixed solvent was 5/5, a relatively low $\delta_{p,s}$ obtained, meaning a stronger interaction between solvent and PVDF, thus a well dissolved system was formed. The $\delta_{p,s}$ of TEP and PVDF was also maintained at low value. In these two cases (M-D5T5 and M-TEP), only α phase existed. It came to a conclusion that greater $\delta_{p,s}$ tended to form β phase while smaller $\delta_{p,s}$ favored the formation of α phase.

Crystalline Structure on Top Surface of PVDF Membrane by FTIR–ATR. Compared to membrane bulk, varied crystalline forms might be obtained on membrane top surface due to polymer concentration gradient. On this account, FTIR–ATR technique was performed. As can be seen in Figure 5, the crystalline structures of top surface mainly coincide with membrane bulk.

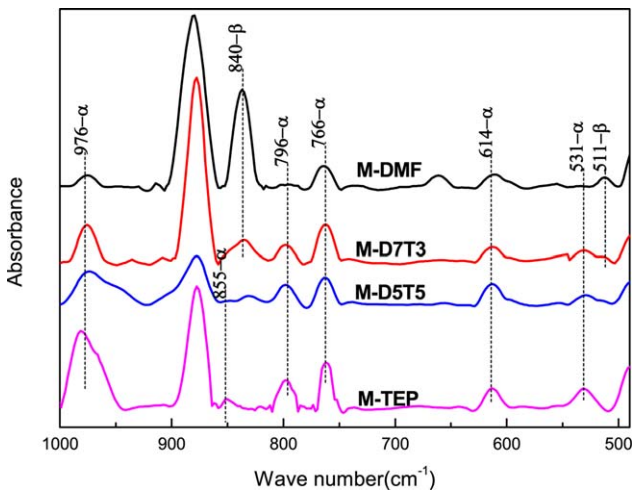

Figure 3. FTIR spectra of M-DMF, M-D7T3, M-D5T5, and M-TEP. [Color figure can be viewed in the online issue, which is available at wileyonlinelibrary.com.]

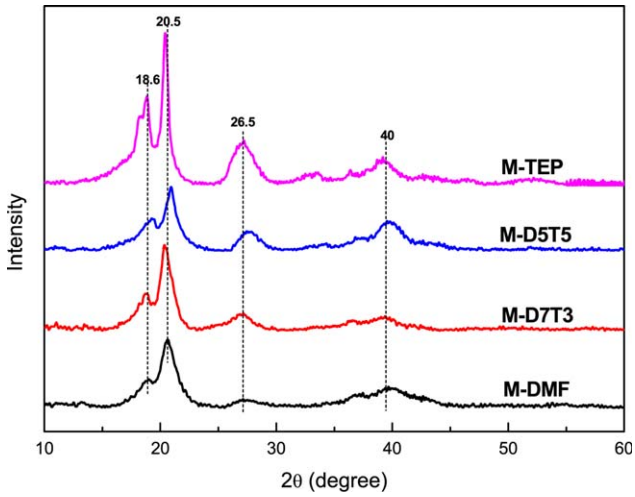

Figure 4. X-ray diffractogram of M-DMF, M-D7T3, M-D5T5, and M-TEP. [Color figure can be viewed in the online issue, which is available at wileyonlinelibrary.com.]

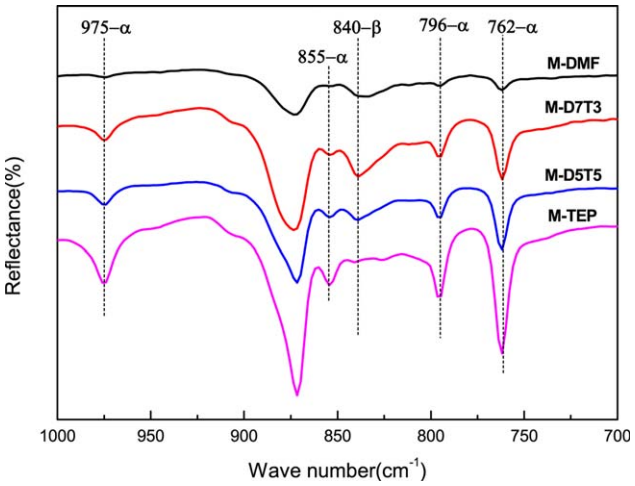

Figure 5. FTIR–ATR spectra of top surface of M-DMF, M-D7T3, M-D5T5, and M-TEP. [Color figure can be viewed in the online issue, which is available at wileyonlinelibrary.com.]

M-D5T5 without β phase in bulk had a weak β signal at 840 cm^{-1} on top surface. Higher polymer concentration on top surface should be responsible for this phenomenon. Since it is widely accepted that higher polymer concentration engendered better oriented packing of CH_2—CF_2 dipoles, consequently some β phase was formed.[37]

Membrane Hydrophilicity and Crystallization Behavior. Membrane hydrophilicity was investigated by contact angle experiment. As shown in Table II, the contact angle of membranes prepared with different solvents varied between 122° and 108°, and no significant correlation with solvent composition was found. Crystallization behavior of PVDF membranes was measured by DSC experiment. The result (Table II) indicted that membranes produced with different solvents obtained a similar melting temperature around 164°C, due to the consistency in melting temperature of α and β phase.[38] However, the crystallinity of membranes with different solvents varied. M-DMF and M-TEP, which were prepared with pure solvents gained lower crystallinity as compared with M-D7T3 and M-D5T5 prepared with mixed solvents. A greater permeation pressure of pure solvent lead to a higher exchange rate between solvent and supercritical CO_2, thus the casting solution could reach solidification region in a short time. In contrast, membranes produced with mixed solvents obtained relatively longer time before solidification, and the crystallization of these membranes could be much completer, the crystallinity of M-D7T3 and M-D5T5 reached 40.8%.

Effect of Salt Additive on Membrane Morphology and Crystallization

In this part, we aimed to make an investigation to understand whether LiCl enhanced β phase of PVDF membrane produced by novel supercritical CO_2 induced phase separation process. Eighteen weight percentage PVDF and varied amount of LiCl (1, 2, and 4 wt %) was dissolved in pure DMF to form a homogeneous casting solution, and the supercritical CO_2 condition was kept at 45°C, 80 bar. The membranes were named as M-1%L, M-2%L, and M-4%L corresponding to the amounts of LiCl added in solution.

Morphology of PVDF Membranes Prepared with Different Amounts of LiCl. LiCl interacts strongly with polar aprotic DMF solvent and form complexes with carbonyl group, this may result in a more favorable membrane morphology.[39]

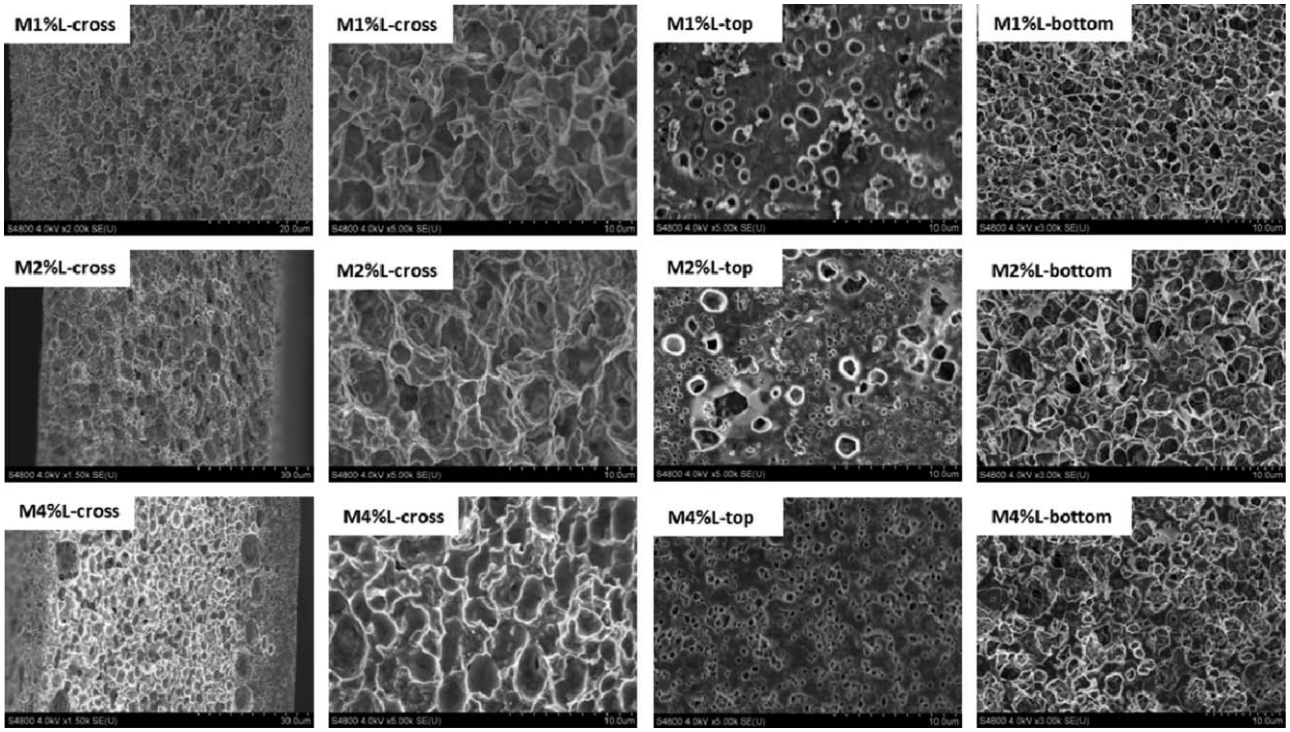

Figure 6. SEM images of cross section and surface structures of M-1%L, M-2%L, and M-4%L.

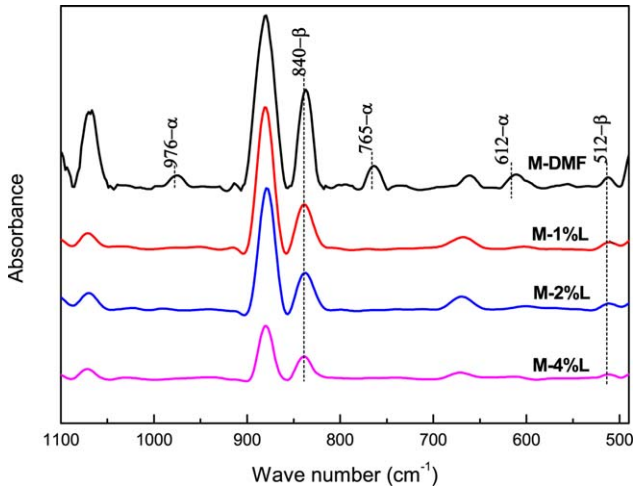

Figure 7. FTIR spectra of M-DMF, M-1%L, M-2%L, and M-4%L. [Color figure can be viewed in the online issue, which is available at wileyonlinelibrary.com.]

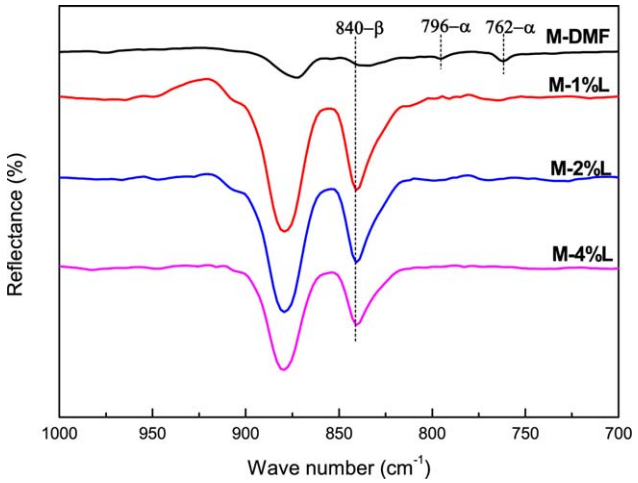

Figure 9. FTIR–ATR spectra of the top surface of M-DMF, M-1%L, M-2%L, and M-4%L. [Color figure can be viewed in the online issue, which is available at wileyonlinelibrary.com.]

Recently, Ismail and coworkers[40,41] have proved that using suitable amount of LiCl as an additive yielded less finger like structure and high surface porosity in hollow fiber PVDF membranes by NIPS method. Figure 6 revealed SEM images of PVDF membranes prepared with different amounts of LiCl, as compared with the membrane (M-DMF) without LiCl, a significant morphology variation was obtained. The addition of LiCl lead to a thermodynamically unstable casting solution, the formation rate of skin layer was enhanced, and the thinner membrane thickness was obtained. The pore size at cross-section was nearly the same regardless of different amounts of LiCl, whereas the pores at top surface varied obviously. When compared to M-1%L and M-2%L, the pore size at top surface of M-4%L decreased dramatically due to the increased viscosity. Moreover, uniform pores were found at bottom surface for all membrane doped LiCl.

Crystalline Structure of PVDF Membrane Bulk. As shown in Figure 7, after adding LiCl, the crystalline phase of PVDF membrane varied significantly in comparison with M-DMF, which obtained a crystalline phase involving with α and β phase. For M-1%L, M-2%L, and M-4%L, FTIR signal corresponding to β phase appeared at 840 and 512 cm^{-1}, while peaks at 976, 765, and 612 cm^{-1} ascribing to α phase completely vanished. The result from XRD (Figure 8) agreed well with FTIR spectra. When LiCl was introduced, shoulder peak at 18.6°, which was associated to reflection of α (020) became indistinct. The peak associated to α (021) phase around 26.5° also disappeared even only one percent of LiCl was introduced. Moreover, peak around 40°, which indicted the combination of α (002) and α (201) turned to be weaker and smoother. Especially for M-4%L prepared with high viscous casting solution, it seemed no evident peak around 40°. Both FTIR and XRD results drew a consequence that addition of LiCl boosted β phase of PVDF membranes.

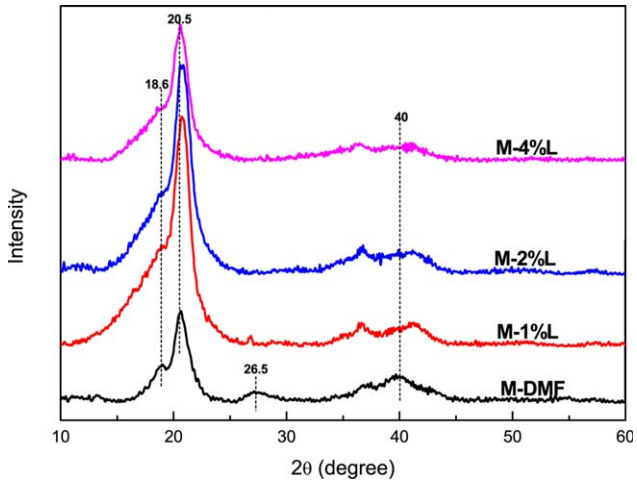

Figure 8. X-ray diffractogram of M-DMF, M-1%L, M-2%L, and M-4%L. [Color figure can be viewed in the online issue, which is available at wileyonlinelibrary.com.]

Crystalline Structure on Top Surface of PVDF Membrane. The crystalline structure of top surface of PVDF membranes prepared with different amounts of LiCl was investigated by FTIR-ATR experiment. From Figure 9, it can be seen that peak at 840 cm^{-1} ascribed to β phase became visibly sharper when LiCl was added, furthermore, α peaks at 792 and 762 cm^{-1} disappeared. The influence of different amounts of LiCl on crystalline structure was not evident.

CONCLUSIONS

In our study, DMF, TEP, and the corresponding mixture with different ratio were applied to reveal the influence of solvent power on PVDF membrane morphology and polymorphism via supercritical CO_2 induced phase separation. It was disclosed that the pore size in cross-section decreased with increasing TEP content. Because of the smaller the difference of solubility parameters ($\delta_{p,s} = 1.06$ $MPa^{1/2}$), a delayed phase separation occurred for M-D5T5 and a denser top surface was obtained. PVDF membrane tended to form α phase with increasing TEP content due to the smaller dipole moment. Addition of LiCl promoted a cellular cross section and more porous top surface,

and enhanced the formation of β phase during supercritical CO_2 induced phase separation.

ACKNOWLEDGMENTS

The authors would like to thank National Natural Science Foundation of China (51273211), National 863 Foundation of China (2012AA03A605), the international cooperation project from Ministry of Science and Technology of China (2012DFR50470).

REFERENCES

1. Liu, F.; Hashim, N. A.; Liu, Y.; Abed, M. R. M.; Li, K. *J. Membr.Sci.* **2011**, *375*, 1.
2. Wang, Q.; Wang, X.; Wang, Z.; Huang, J.; Wang, Y. *J. Membr. Sci.* **2013**, *442*, 57.
3. Reverchon, E.; Cardea, S. *Ind. Eng. Chem. Res.* **2006**, *45*, 8939.
4. Cardea, S.; Sessa, M.; Reverchon, E. *Soft Mater.* **2011**, *9*, 264.
5. Sairiam, S.; Loh, C. H.; Wang, R.; Jiraratananon, R. *J. Appl. Polym. Sci.* **2013**, *130*, 610.
6. Zhang, P.-Y.; Yang, H.; Xu, Z.-L.; Wei, Y.-M.; Guo, J.-L.; Chen, D.-G. *J. Polym. Res.* **2013**, *20*.
7. Cho, I. S.; Kim, J. H.; Kim, S. S. *Korea Polym. J.* **1997**, *5*, 191.
8. Tomasko, D. L.; Li, H. B.; Liu, D. H.; Han, X. M.; Wingert, M. J.; Lee, L. J.; Koelling, K. W. *Ind. Eng. Chem. Res.* **2003**, *42*, 6431.
9. Davies, O. R.; Lewis, A. L.; Whitaker, M. J.; Tai, H.; Shakesheff, K. M.; Howdle, S. M. *Adv. Drug Deliv. Rev.* **2008**, *60*, 373.
10. Duarte, A. R. C.; Mano, J. F.; Reis, R. L. *J. Bioact. Compat. Polym.* **2009**, *24*, 385.
11. Noyori, R. *Chem. Rev.* **1999**, *99*, 353.
12. Cardea, S.; Sessa, M.; Reverchon, E. *Ind. Eng. Chem. Res.* **2010**, *49*, 2783.
13. Hirschinger, J.; Schaefer, D.; Spiess, H. W.; Lovinger, A. J. *Macromolecules* **1991**, *24*, 2428.
14. Lovinger, A. J. *Macromolecules* **1982**, *15*, 40.
15. McFee, J. H.; Bergman, J. G.; Crane, G. R. *Ferroelectrics* **1972**, *3*, 305.
16. Furukawa, T. *IEEE. Trans. Electr Insul.* **1989**, *24*, 375.
17. Zhao, X. Z.; Bharti, V.; Zhang, Q. M.; Romotowski, T.; Tito, F.; Ting, R. *Appl. Phys. Lett.* **1998**, *73*, 2054.
18. Tao, M.-M.; Liu, F.; Ma, B.-R.; Xue, L.-X. *Desalination* **2013**, *316*, 137.
19. Lin, D. J.; Chang, C. L.; Huang, F. M.; Cheng, L. P. *Polymer* **2003**, *44*, 413.
20. Kepler, R. G.; Anderson, R. A. *Adv. Phys.* **1992**, *41*, 1.
21. Wang, J. J.; Li, H. H.; Liu, J. C.; Duan, Y. X.; Jiang, S. D.; Yan, S. K. *J. Am. Chem. Soc.* **2003**, *125*, 1496.
22. Fontananova, E.; Jansen, J. C.; Cristiano, A.; Curcio, E.; Drioli, E. *Desalination* **2006**, *192*, 190.
23. Gregorio, R., Jr.; Borges, D. S. *Polymer* **2008**, *49*, 4009.
24. Matsuyama, H.; Yamamoto, A.; Yano, H.; Maki, T.; Teramoto, M.; Mishima, K.; Matsuyama, K. *J. Membr. Sci.* **2002**, *204*, 81.
25. Matsuyama, H.; Yano, H.; Maki, T.; Teramoto, M.; Mishima, K.; Matsuyama, K. *J. Membr. Sci.* **2001**, *194*, 157.
26. Boccaccio, T.; Bottino, A.; Capannelli, G.; Piaggio, P. *J. Membr. Sci.* **2002**, *210*, 315.
27. Lin, D.-J.; Chang, C.-L.; Lee, C.-K.; Cheng, L.-P. *Eur. Polym. J.* **2006**, *42*, 2407.
28. Groning, R.; Braun, F. J. *Pharmazie* **1996**, *51*, 337.
29. Van Krevelen, D.; Nijenhuis, K. Elsevier: New York, **1990**.
30. Bottino, A.; Cameraroda, G.; Capannelli, G.; Munari, S. *J. Membr. Sci.* **1991**, *57*, 1.
31. Kim, J. H.; Min, B. R.; Won, J.; Park, H. C.; Kang, Y. S. *J. Membr. Sci.* **2001**, *187*, 47.
32. Wang, L. J.; Li, Z. S.; Ren, J. Z.; Li, S. G.; Jiang, C. Z. *J. Membr. Sci.* **2006**, *275*, 46.
33. Wang, Q.; Wang, Z.; Wu, Z. *Desalination* **2012**, *297*, 79.
34. Shen, F.; Lu, X. F.; Bian, X. K.; Shi, L. Q. *J. Membr. Sci.* **2005**, *265*, 74.
35. He, X.; Yao, K. *Appl. Phys. Lett.* **2006**, 89.
36. Benz, M.; Euler, W. B.; Gregory, O. J. *Langmuir* **2001**, *17*, 239.
37. Zhang, M.; Zhang, A.-Q.; Zhu, B.-K.; Du, C.-H.; Xu, Y.-Y. *J. Membr. Sci.* **2008**, *319*, 169.
38. Gregorio, R.; Cestari, M. *J. Polym. Sci. Part B: Polym.Phys.* **1994**, *32*, 859.
39. Lee, H. J.; Won, J.; Lee, H.; Kang, Y. S. *J. Membr. Sci.* **2002**, *196*, 267.
40. Naim, R.; Ismail, A. F.; Mansourizadeh, A. *J. Membr. Sci.* **2012**, *392*, 29.
41. Mansourizadeh, A.; Ismail, A. F. *Chem. Eng. J.* **2010**, *165*, 980.